PHYSICAL REVIEW B **92**, 201413(R) (2015)

Structural evolution and optoelectronic applications of multilayer silicene

Zhi-Xin Guo,[1,*] Yue-Yu Zhang,[2] Hongjun Xiang,[2] Xin-Gao Gong,[2] and Atsushi Oshiyama[3]

[1]*Department of Physics, Xiangtan University, Xiangtan, Hunan 411105, China*

[2]*Key Laboratory of Computational Physical Sciences (Ministry of Education), State Key Laboratory of Surface Physics, Collaborative Innovation Center of Advanced Microstructures, and Department of Physics, Fudan University, Shanghai 200433, China*

[3]*Department of Applied Physics, The University of Tokyo, Hongo, Tokyo 113-8656, Japan*

(Received 18 August 2015; revised manuscript received 13 October 2015; published 25 November 2015)

Despite the recent progress on two-dimensional multilayer materials (2DMMs) with weak interlayer interactions, the investigation of 2DMMs with strong interlayer interactions is far from sufficient. Here, we report on first-principles calculations that clarify the structural evolution and optoelectronic properties of such a 2DMM, multilayer silicene. With our global optimization algorithm, we discover the existence of rich dynamically stable multilayer silicene phases, whose stability is closely related to the extent of sp^3 hybridization that can be evaluated by average bonds and effective bond angles. Stable Si(111) surface structures are obtained when the silicene thickness gets up to four, showing the critical thickness for a structural evolution. We also find that multilayer silicene with π-bonded surfaces presents outstanding optoelectronic properties for solar cells and optical fiber communications due to the incorporation of sp^2-type bonds in the sp^3-type bond dominated system. This study helps to complete the picture of the structure and related property evolution of 2DMMs with strong interlayer interactions.

DOI: 10.1103/PhysRevB.92.201413 PACS number(s): 73.22.−f, 78.20.Ci, 81.05.Zx, 88.40.jj

Two-dimensional multilayer material (2DMM) is a type of important nanomaterial. By far, 2DMMs with weak interlayer interactions, such as graphene, MoS_2, black phosphorus, etc., have been extensively investigated for their fascinating properties [1–3], whereas those with strong interlayer interactions have been barely explored. The two-dimensional structure of Si (silicene), which has been both theoretically predicted and experimentally synthesized [4–14], can be an ideal material for such an investigation. Despite extensive studies on monolayer silicene [15–20], the investigation of multilayer silicene is far from sufficient. Although a few theoretical investigations have been performed on freestanding bilayer silicene [21–25], the mechanism for relative stability among the obtained phases has not been understood. Moreover, bilayer silicene can be either a metal or semiconductor depending on the specific stacking structures [22–25], while the underlying mechanisms have not been clarified. Also, the structural and electronic properties of thicker freestanding multilayer silicene are still to be explored.

On the other hand, Si surfaces are premier stages on which the fabrication of most electron devices is achieved. The atomic layers of Si(111) surfaces have a hexagonal network in the lateral plane, and thus the similarities and dissimilarities between multilayer silicene and the surface atomic layers of Si(111) surfaces are intriguing. Actually, the cleaved Si(111) surface shows 2×1 periodicity and then its annealing converts it to a more stable 7×7 periodicity. The 2×1 phase has been identified as a π-bonded chain structure [26] and a dimer-adatom-stacking-fault (DAS) model [27,28] is now established for the 7×7 phase [29,30]. It is important and interesting to clarify the structural evolution between the silicene and reconstructed surface phases in multilayer Si.

Although the majority of solar cells fabricated to date have been based on three-dimensional (3D) Si, it is well known that 3D Si is not an ideal material for optoelectronic applications due to its large direct band gap (3.4 eV [31]). Because of excellent compatibility with the mature Si-based microelectronics industry and a high abundance of Si, the discovery of multilayer silicene materials with excellent optoelectronic properties may lead to a revolution in future optoelectronics technology.

In this Rapid Communication, by performing extensive calculations for multilayer silicene from bilayers to quadlayers, we clarify the structural evolution and the outstanding optoelectronic properties of multilayer silicene. Searches for stable multilayer silicene phases are performed using our global optimization algorithm code (IM^{2}ODE [32]), which was developed based on differential evolution. We consider structures with a different number n of Si atoms in the unit cell ($2 \leqslant n \leqslant 36$). The population size is set to be 20 and the number of generations is fixed at 15 in the usual cases. The structural relaxations are performed using the Vienna *ab initio* simulation package (VASP) [33]. The stability of the obtained phases is verified by phonon calculations [37]. The final accurate calculations of the energy bands and optical spectra are performed using the Heyd-Scuseria-Ernzerhof (HSE06) functional as implemented in VASP.

With the IM^{2}ODE code, we have performed extensive searches for the most stable phases of silicene from the monolayer to quadlayer. We have obtained several different monolayer silicene phases (Fig. S1 [38]) which are energetically stable to the well-known low-buckled honeycomb phase [4], but they are unstable from the phonon calculations. This shows that the low-buckled honeycomb structure is the most stable monolayer silicene phase.

The most stable bilayer silicene phase we have obtained is the hex-OR-2×2 structure with the cohesive energy (E_c) being 5.073 eV/Si [Fig. S2(a)] [38], which is the same as that obtained in previous work using the structural exploration method [24]. Since this phase presents the P-1 symmetry, here we denote it as the P-1-2×2 phase. We have also reached

*zxguo08@hotmail.com

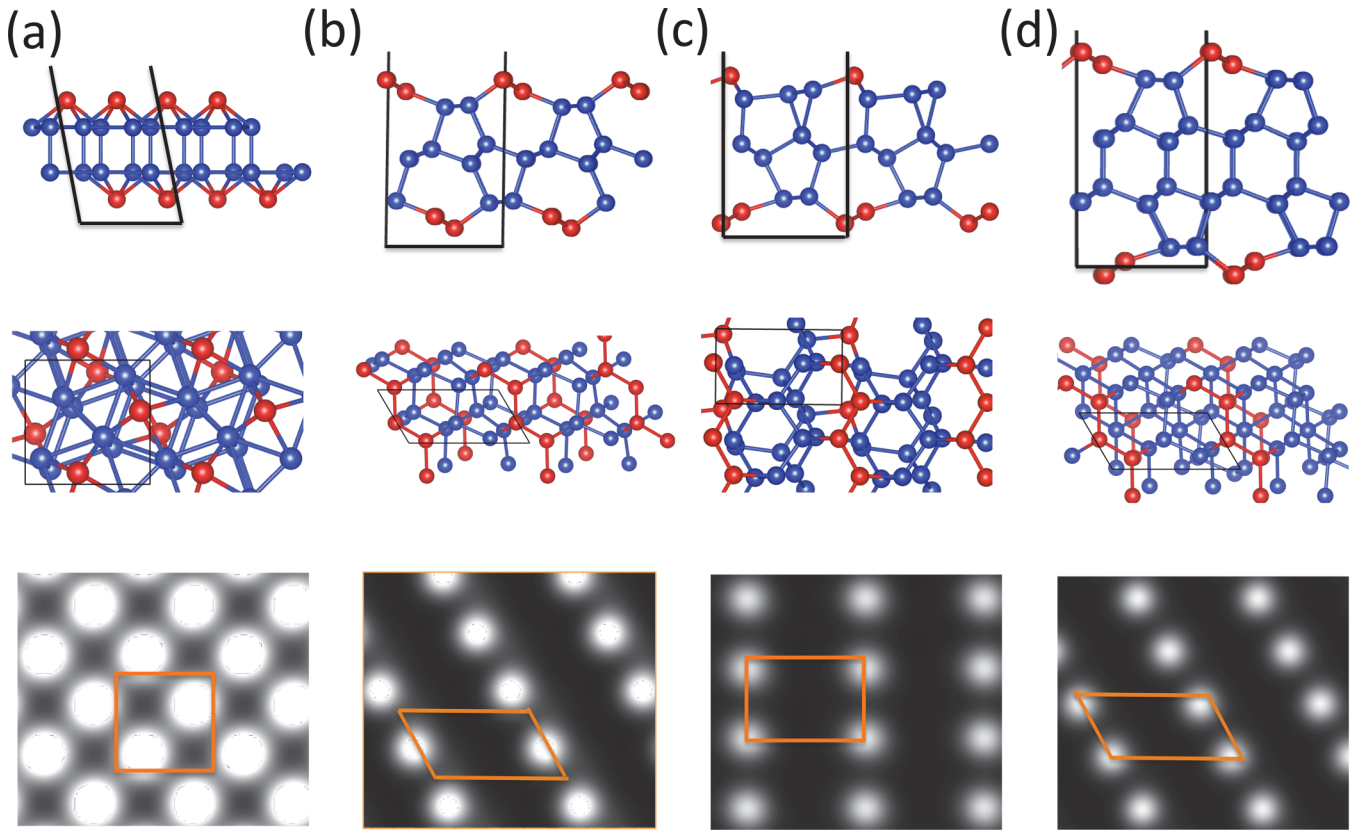

FIG. 1. (Color online) Side (upper panels) and top (middle panels) views of the stable phases of freestanding multilayer silicene and corresponding occupied STM images (bottom panels). (a) $C12/m1$–$\sqrt{2}\times\sqrt{2}$ bilayer silicene, (b) $P121/m1$–2×1 and (c) $P1$–2×1 trilayer silicene, and (d) $P1m1$–2×1 quadlayer silicene. The highly protruded Si atoms at the surfaces are depicted by the red balls and the remaining Si atoms are depicted by the blue balls. The lateral unit cells are also indicated by the solid lines.

the slide-2×2 ($E_c = 5.063$ eV/Si) and $Cmme$–1×1 ($E_c = 5.000$ eV/Si) phases as previously reported [23,24], which are the second most stable and the most stable phases with periodicities of 2×2 and 1×1, respectively [Figs. S2(b) and S2(c)] [38]. The slide-2×2 phase has $C12/m1$ symmetry, thus it is denoted as the $C12/m1$–2×2 phase accordingly. Additionally, we have obtained a phase which presents the $C12/m1$ symmetry with a periodicity of $\sqrt{2}\times\sqrt{2}$ ($E_c = 4.991$ eV/Si, denoted as $C12/m1$–$\sqrt{2}\times\sqrt{2}$) [Fig. 1(a)]. The four bilayer silicene phases are dynamically stable, as evidenced from the calculated phonon spectra shown in Fig. S3(a) [38] as well as in Ref. [24]. The cohesive energies of the bilayer silicene phases are larger than the monolayer silicene by 240–320 meV/Si, showing covalent interlayer interactions. The above results show the existence of rich stable bilayer silicene phases. The calculated occupied scanning tunneling microscopy (STM) [39] images of the four bilayer silicene phases are different from each other with different periodicities, i.e., hexagonal, tetragonal, and rhombic geometries for the 1×1, $\sqrt{2}\times\sqrt{2}$, and 2×2 phases, respectively, which make them easily distinguishable in experiments. Whereas the two rhombic STM images of the P-1-2×2 and $C12/m1$–2×2 phases are very similar, additional techniques have to be used to distinguish them.

To explore the structural evolution in multilayer silicene, we have also performed extensive searches for stable trilayer silicene phases. Several stable phases have been obtained, where the two most stable present a 2×1 periodicity with hexagonal ($E_c = 5.138$ eV/Si) and rectangular supercells ($E_c = 5.135$ eV/Si) [Figs. 1(b) and 1(c)], respectively. Their dynamical stability has also been verified by phonon calculations [Figs. S3(b) and S3(c)] [38]. The hexagonal and rectangular phases have $P121/m1$ and $P1$ symmetries, so they are thus denoted as $P121/m1$–2×1 and $P1$–2×1, respectively. Particularly, in the $P121/m1$–2×1 phase, the top (bottom) silicene layer is drastically reconstructed to form chains of π orbitals associated with the five- and seven-membered rings of the top (bottom) and middle silicene layers. This feature is the same as that of the 2×1 Si(111) surface, but there is an obvious distortion in the middle silicene layer with respect to the second Si layer [40] of the 2×1 Si(111) surface [26]. The structure of the $P1$–2×1 phase is similar to the $P121/m1$–2×1 phase. The difference mainly lies in the fact that the seven-membered ring in the $P121/m1$–2×1 phase splits into three-membered and six-membered rings in the $P1$–2×1 phase. The calculated occupied STM images of both phases are shown in Figs. 1(b) and 1(c), which present the atomic chain image as that of the 2×1 Si(111) surface. We have also verified the stability of the trilayer 7×7 silicene phase with the initial surface structure being the same as the 7×7 Si(111) surface with the DAS model [27,28]. After geometry optimization, however, the geometry is very much distorted. This shows that trilayer silicene is too thin to reproduce the complex 7×7 Si(111) surface structure.

TABLE I. Geometry symmetry, cohesive energy E_c (eV/Si), average bond number (ABN), average effective bond angle normalized with respect to 109.47° (AEBA1) and 120° (AEBA2), as well as a direct band gap (DBG) in units of eV for monolayer (ML), bilayer (BL), trilayer (TL), and quadlayer (QL) silicene.

	Periodicity	Symmetry	E_c	ABN	AEBA1	AEBA2	DBG
ML	1×1	$P6/mm$	4.750	3.00	0.94	0.96	
BL	1×1	$Cmme$	5.000	4.00	0.87	0.83	
BL	$\sqrt{2}\times\sqrt{2}$	$C12/m1$	4.991	4.00	0.85	0.82	
BL	2×2	P-1	5.073	3.75	0.89	0.86	1.5
BL	2×2	$C12/m1$	5.063	3.75	0.88	0.86	0.5
TL	2×1	$P121/m1$	5.138	3.67	0.93	0.90	0.5
TL	2×1	$P1$	5.135	3.83	0.91	0.88	0.9
QL	2×1	$P1m1$	5.225	3.75	0.94	0.90	0.7

We have then explored the stable phases for the thicker silicene, i.e., the quadlayer silicene. With the IM^{2}ODE code, we have obtained several stable phases, among which the 2×1 phase with $P1m1$ symmetry is the most stable with $E_c = 5.225$ eV/Si [denoted as $P1m1{-}2\times1$, Fig. 1(d)]. The top and bottom two silicene layers in this phase present the perfect π-bonded chain structure, whose geometries resemble 2×1 Si(111) surfaces with positive and negative buckling reconstructions [41], respectively. The dynamical stability of the 2×1 silicene phase is verified by phonon calculations [Fig. S3(d)] [38]. We have also verified the stability of the 7×7 DAS structure following the way in trilayer silicene. After geometry optimization, a stable 7×7 DAS structure is obtained in quadlayer silicene [Fig. S2(d)]. The simulated occupied STM images of the 2×1 [Fig. 1(d)] and 7×7 [Fig. S2(d)] [38] silicene phases confirm their structural similarity to those of the Si(111) surfaces. The E_c of the stable 7×7 phase is 5.245 eV/Si, 20 meV/Si larger than the 2×1 phase. This is consistent with the fact that the 7×7 reconstruction is more stable than the 2×1 reconstruction in Si(111). The above results show that the quadlayer is the critical thickness for a structural transition from silicene to a Si(111) surface.

Although multilayer silicene phases are rich and complex, their structures can be roughly characterized by using an average bond number (ABN) [42] and average effective bond angle (AEBA) [43]. For instance, the ABN in both $Cmme{-}1\times1$ and $C12/m1{-}\sqrt{2}\times\sqrt{2}$ bilayer silicene is 4.00 since all the Si atoms are fourfold coordinated, whereas it is 3.75 in P-1-2×2 and $C12/m1{-}2\times2$ bilayer silicene since 25% Si atoms are threefold coordinated and the remaining 75% Si atoms are fourfold coordinated (Table I). The AEBA can be normalized with respect to the ideal sp^3 (AEBA1) and sp^2 (AEBA2) bond angles, which are 109.47° and 120°, respectively [43]. From Table I, for all multilayer silicene phases, the ABN is larger than 3.50 and the AEBA1 is larger than AEBA2. This feature shows that the majority of Si atoms are fourfold coordinated and the bond angles are closer to the sp^3 type, reflecting the nature of sp^3-like hybridization in multilayer silicene. It is noteworthy that the ABN equals 3.00 and the AEBA1 is smaller than AEBA2 in monolayer silicene, showing the nature of sp^2-like hybridization.

The cohesive energy E_c is summarized in Table I to show the stability of the silicene phases. A common feature is that E_c increases with increasing silicene thickness, which is 240–480 meV/Si stable to the monolayer silicene. This shows that thicker silicene is more easily obtained in experiments. It is noticed that P-1-2×2 and $C12/m1{-}2\times2$ bilayer silicenes are more stable than $Cmme{-}1\times1$ and $C12/m1{-}\sqrt{2}\times\sqrt{2}$ bilayer silicenes by 60–70 meV/Si, which is unexpected since the ABN is smaller by 0.25 bond per Si in the two former phases. This is mainly owing to the different bond angle distributions, which affect the strength of $s-p$ hybridizations and thus the bond energies. The AEBA1 is larger in the two 2×2 phases than those in the 1×1 and $\sqrt{2}\times\sqrt{2}$ phases, showing that the structural characteristics in the 2×2 phases are closer to the diamond Si, which is the most stable Si phase. A similar tendency is also obtained in thicker silicene phases (Table I). These results imply a general rule for the stability of dynamically stable multilayer silicene with similar ABN values, i.e., silicene phases with larger AEBA1 values are usually more stable.

The electronic properties of the multilayer silicene phases are further calculated. It is found that $Cmme{-}1\times1$ and $C12/m1{-}\sqrt{2}\times\sqrt{2}$ bilayer silicenes are metallic (Fig. S4) [38], whereas the P-1-2×2 and $C12/m1{-}2\times2$ bilayers, the $P121/m1{-}2\times1$ and $P1{-}2\times1$ trilayers, as well as the $P1m1{-}2\times1$ quadlayer silicene are indirect semiconductors with the band gaps varying from 0.4 to 1.3 eV (Fig. 2). From the structural details, the $s-p$ orbital hybridizations in the two former metallic phases are much distorted from the ideal sp^3 hybridization, although all the Si atoms are fourfold coordinated. As for the four latter semiconductor phases, however, the hybridizations of threefold-coordinated and fourfold-coordinated Si atoms resembling the sp^2 and sp^3 hybridizations, respectively. The different forms of orbital hybridizations in the multilayer silicene induce very different electronic properties. These results indicate that the electronic properties of multilayer silicene can be effectively manipulated by structural engineering. On the other hand, the direct band gaps (DBGs) of these indirect semiconductor silicene phases are in range of 0.5–1.5 eV (Table I), which are very close to their indirect band gaps. This implies their outstanding optoelectronic properties for applications in optical fiber communications and solar cells, where the required optimal band gaps are 0.8 and 1.5 eV, respectively.

It is well known that the imaginary part of the dielectric tensor ε_2 determines the absorption ability of a material. The calculated ε_2 of the semiconductor multilayer silicene phases are shown in Fig. S5 [38]. After careful analyses, it is found that the optical absorptions in all these phases start at the direct band gap. This implies that the P-1-2×2 bilayer silicene (DBG = 1.5 eV) and $P1{-}2\times1$ trilayer silicene (DBG = 0.9 eV) are suitable for solar cells according to the Shockley-Queisser limit [44], whereas $C12/m1{-}2\times2$ bilayer silicene (DBG = 0.5 eV), $P121/m1{-}2\times1$ trilayer silicene (DBG = 0.5 eV), and $P1m1{-}2\times1$ quadlayer silicene (DBG = 0.7 eV) are suitable for fiber communications.

We have further calculated the optical absorption coefficients of semiconductor multilayer silicene phases and compared them with that of GaAs, whose conversion efficiency is the highest among all thin-film solar cell absorbers. As shown in Fig. 3(a), the optical absorption coefficients of P-1-2×2 bilayer silicene and $P1{-}2\times1$ trilayer silicene are up to

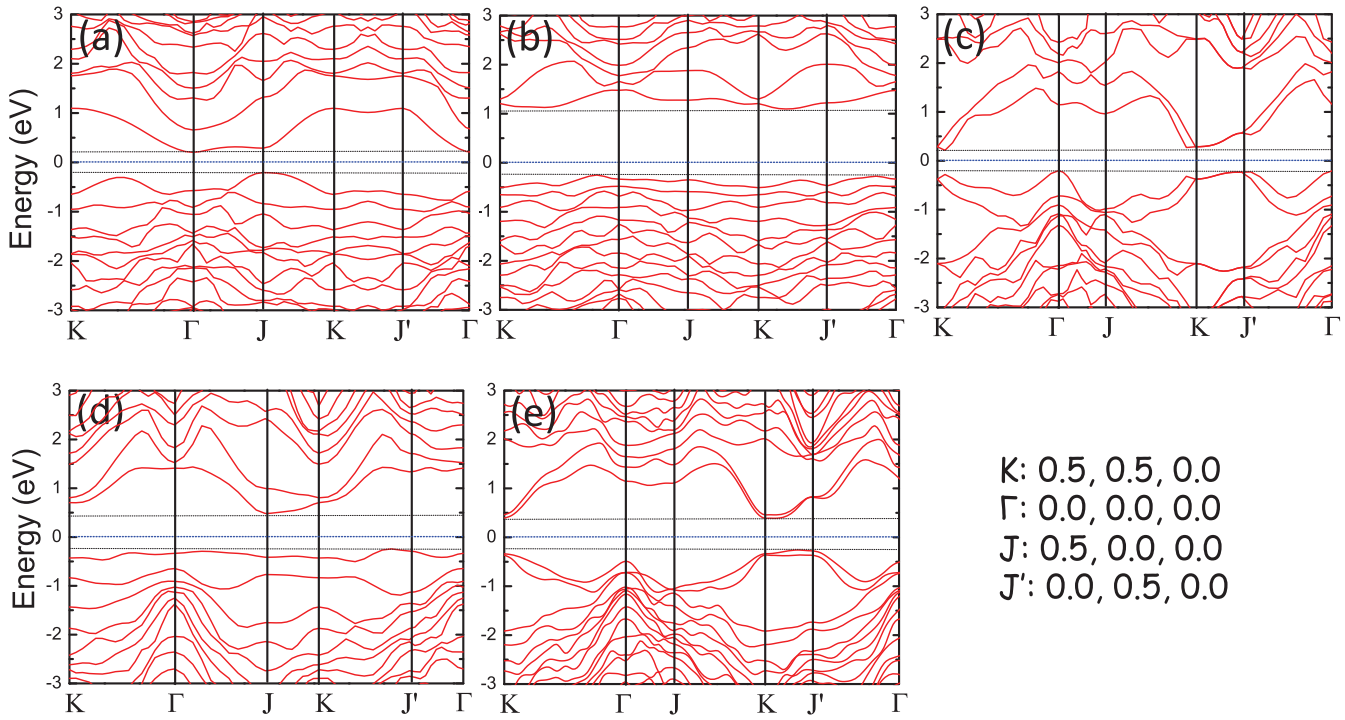

FIG. 2. (Color online) Calculated energy bands of semiconductor multilayer silicene. Energy bands of (a) $C12/m1{-}2 \times 2$ bilayer silicene, (b) P-1-2 $\times$ 2 bilayer silicene, (c) $P121/m1{-}2 \times 1$ trilayer silicene, (d) $P1{-}2 \times 1$ trilayer silicene, and (e) $P1m1{-}2 \times 1$ quadlayer silicene. The valence band maximum (VBM) and conduction band minimum (CBM) are indicated by the short-dotted black lines.

$\sim 10^5$ cm^{-1}, one order of magnitude higher than that of GaAs in the energy range of about 1.0–2.0 eV, showing that they are very good nanoscale solar cell absorbers. On the other hand, the absorption coefficients of $P121/$m1-2 $\times$ 1 trilayer silicene and $P1m1{-}2 \times 1$ quadlayer silicene are also up to $\sim 10^5$ cm^{-1} in an energy range of 0.5–1.0 eV [Fig. 3(b)], showing that they are good for nanoscale fiber communications. The absorption coefficient of $C12/m1{-}2 \times 2$ bilayer silicene is one order smaller [Fig. 3(b)], indicating that it is not suitable for optical applications.

To explore the mechanism of the outstanding optoelectronic properties of multilayer silicene, we have analyzed their corresponding optical transition matrix and their energy bands. It is found that the absorption peaks with a photon energy smaller than 2.0 (1.0) eV for P-1-2 $\times$ 2 bilayer silicene and $P1{-}2 \times 1$ trilayer silicene ($P121/m1{-}2 \times 1$ trilayer silicene and $P1m1{-}2 \times 1$ quadlayer silicene) are mainly attributed to the transitions between the first two valence and conduction bands, especially along the K-J' direction in the Brillouin zone. The Kohn-Sham (KS) orbitals (Fig. 4) further show that these energy bands mainly come from the p_z (π) orbitals of the Si atoms at silicene surfaces, which present sp^2 hybridization. Similar results have also been found in thicker silicene phases, i.e., the six- and eight-Si-layered

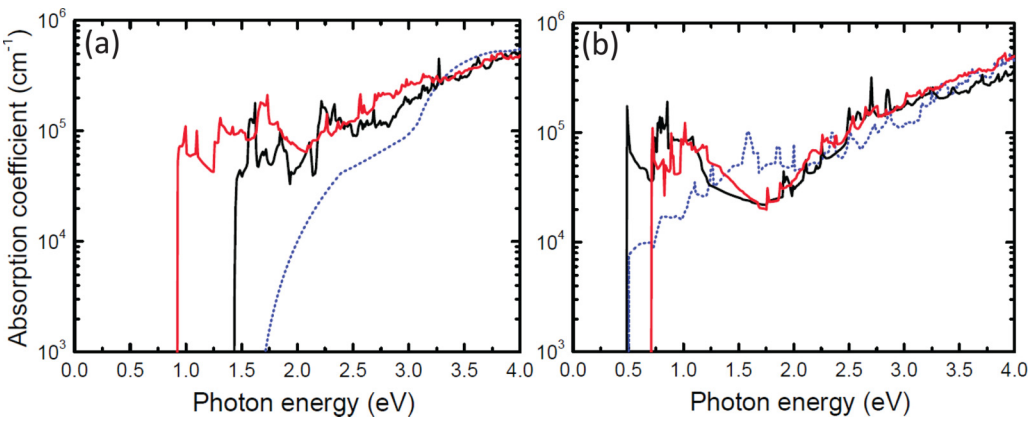

FIG. 3. (Color online) Comparison of the calculated optical absorption coefficients of multilayer silicene with GaAs. (a) Optical absorption coefficients of P-1-2 $\times$ 2 bilayer silicene (solid black line), $P1{-}2 \times 1$ trilayer silicene (solid red line), and bulk GaAs (short-dotted blue line). (b) Optical absorption coefficients of $C12/m1{-}2 \times 2$ bilayer silicene (short-dotted blue line), $P121/m1{-}2 \times 1$ trilayer silicene (solid black line), and $P1m1{-}2 \times 1$ quadlayer silicene (solid red line).

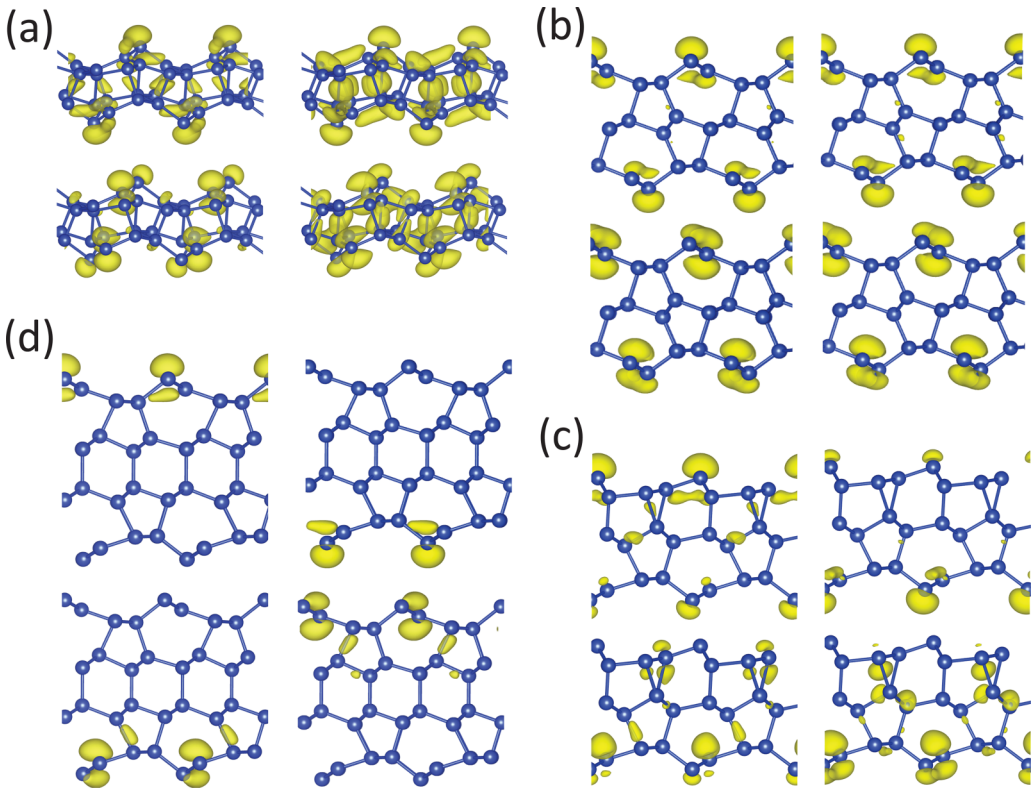

FIG. 4. (Color online) Squared Kohn-Sham (KS) orbitals of the first two valence (upper panels) and conduction (bottom panels) bands shown in Fig. 2 at the K point in the Brillouin zone for (a) P-1-2 $\times$ 2 bilayer silicene [Fig. 2(b)], (b) $P121/m1-2 \times 1$ trilayer silicene [Fig. 2(c)], (c) $P1-2 \times 1$ trilayer silicene [Fig. 2(d)], and (d) $P1m1-2 \times 1$ quadlayer silicene [Fig. 2(e)]. The isovalue surface of the squared KS orbital is taken as 30% of the maximum value.

2×1 silicene (Fig. S6 [38]). These results clearly show that the promising optical properties of these multilayer silicene phases are induced by the incorporation of sp^2 hybridization. It is known that the materials consisting of pure sp^2-type (such as monolayer graphene, silicene) and sp^3-type (such as diamond C, Si) bonds with group IV elements usually have direct band gaps that are too small and too large for optoelectronic applications, respectively. A common feature of multilayer silicene phases with appropriate direct band gaps is the existence of some sp^2-type bonds in the sp^3-type bond dominated system. This kind of configuration can therefore overcome the deficiency of the energy bands of a monotonous $s-p$ hybridized system.

In conclusion, by combining our global optimization algorithm with first-principles calculations, we have discovered many dynamically stable multilayer silicene phases with different thicknesses and have explored the mechanism for its relative stability. We have clarified that the quadlayer is the critical thickness for a structural evolution from silicene to Si(111). Finally, we have found that multilayer silicene with π-bonded surfaces presents outstanding optoelectronic properties due to the incorporation of sp^2-type bonds in the sp^3-type bond dominated system, which makes material design for optoelectronic devices more efficient. These findings are also helpful to complete the picture of the structure and related property evolution for strong interlayer-interacted 2DMMs.

We acknowledge Wei Luo for helpful discussions. Work at Xiangtan was supported by NSFC (Grant No. 11204259)and the NSF of Hunan Province (Grant No. 2015JJ6106); work at Fudan was supported by NSFC, Special Funds for Major State Basic Research; work at Tokyo was supported by the research project "Materials Design through Computics" (http://computics-material.jp/index-e.html) by MEXT and the "Computational Materials Science Initiative" by MEXT, Japan.

[1] A. H. Castro Neto, F. Guinea, N. M. R. Peres, K. S. Novoselov, and A. K. Geim, Rev. Mod. Phys. **81**, 109 (2009).

[2] S. Das, H.-Y. Chen, A. V. Penumatcha, and J. Appenzeller, Nano Lett. **13**, 100 (2013).

[3] L. Li, Y. Yu, G. J. Ye, Q. Ge, X. Ou, H. Wu, D. Feng, X. H. Chen, and Y. Zhang, Nat. Nanotechnol. **9**, 372 (2015).

[4] S. Cahangirov, M. Topsakal, E. Aktürk, H. Sąhin, and S. Ciraci, Phys. Rev. Lett. **102**, 236804 (2009).

[5] P. Vogt, P. De Padova, C. Quaresima, J. Avila, E. Frantzeskakis, M. C. Asensio, A. Resta, B. Ealet, and G. Le Lay, Phys. Rev. Lett. **108**, 155501 (2012).

[6] C. L. Lin, R. Arafune, K. Kawahara, N. Tsukahara, E. Minamitani, Y. Kim, N. Takagi, and M. Kawai, Appl. Phys. Express **5**, 045802 (2012).

[7] A. Fleurence, R. Friedlein, T. Ozaki, H. Kawai, Y. Wang, and Y. Yamada-Takamura, Phys. Rev. Lett. **108**, 245501 (2012).

[8] B. Feng, Z. Ding, S. Meng, Y. Yao, X. He, P. Cheng, L. Chen, and K. Wu, Nano Lett. **12**, 3507 (2012).

[9] L. Chen, C.-C. Liu, B. Feng, X. He, P. Cheng, Z. Ding, S. Meng, Y. Yao, and K. Wu, Phys. Rev. Lett. **109**, 056804 (2012).

[10] L. Meng, Y. Wang, L. Zhang, S. Du, R. Wu, L. Li, Y. Zhang, G. Li, H. Zhou, W. A. Hofer, and H.-J. Gao, Nano Lett. **13**, 685 (2013).

[11] P. De Padova, P. Vogt, A. Resta, J. Avila, I. Razado-Colambo, C. Quaresima, C. Ottaviani, B. Olivieri, T. Bruhn, T. Hirahara, T. Shirai, S. Hasegawa, M. C. Asensio, and G. Le Lay, Appl. Phys. Lett. **102**, 163106 (2013).

[12] Z.-X. Guo, S. Furuya, J.-I. Iwata, and A. Oshiyama, J. Phys. Soc. Jpn. **82**, 063714 (2013).

[13] Z.-X. Guo, S. Furuya, J.-I. Iwata, and A. Oshiyama, Phys. Rev. B **87**, 235435 (2013).

[14] Z. L. Liu, M. X. Wang, J. P. Xu, J. F. Ge, G. le Lay, P. Vogt, D. Qian, C. L. Gao, C. Liu, and J. F. Jia, New J. Phys. **16**, 075006 (2014).

[15] C. C. Liu, W. Feng, and Y. Yao, Phys. Rev. Lett. **107**, 076802 (2011).

[16] M. Ezawa, Phys. Rev. Lett. **109**, 055502 (2012).

[17] Z. Ni, Q. Liu, K. Tang, J. Zheng, J. Zhou, R. Qin, Z. Gao, D. Yu, and J. Lu, Nano Lett. **12**, 113 (2012).

[18] L. Pan, H. J. Liu, X. J. Tan, H. Y. Lv, J. Shi, X. F. Tang, and G. Zheng, Phys. Chem. Chem. Phys. **14**, 13588 (2012).

[19] L. Tao, E. Cinquanta, D. Chiappe, C. Grazianetti, M. Fanciulli, M. Dubey, A. Molle, and D. Akinwande, Nat. Nanotechnol. **10**, 227 (2015).

[20] H. Oughaddou, H. Enriquez, M. R. Tchalala, H. Yildirim, A. J. Mayne, A. Bendounan, G. Dujardin, M. A. Ali, and A. Kara, Prog. Surf. Sci. **90**, 46 (2015).

[21] J. Bai, H. Tanaka, and X. C. Zeng, Nano Res. **3**, 694 (2010).

[22] H. Fu, J. Zhang, Z. Ding, H. Li, and S. Meng, Appl. Phys. Lett. **104**, 131904 (2014).

[23] W. Luo, Y. Ma, X. Gong, and H. Xiang, J. Am. Chem. Soc. **136**, 15992 (2014).

[24] Y. Sakai and A. Oshiyama, Phys. Rev. B **91**, 201405 (2015).

[25] F. Liu, C.-C. Liu, K. Wu, F. Yang, and Y. Yao, Phys. Rev. Lett. **111**, 066804 (2013).

[26] K. C. Pandey, Phys. Rev. Lett. **47**, 1913 (1981).

[27] K. Takayanagi, Y. Tanishiro, M. Takahashi, and A. Takahashi, J. Vac. Sci. Technol. B **4**, 1079 (1985).

[28] K. Takayanagi, Y. Tanishiro, M. Takahashi, and A. Takahashi, Surf. Sci. **164**, 367 (1985).

[29] I. Štich, M. C. Payne, R. D. King-Smith, J.-S. Lin, and L. J. Clarke, Phys. Rev. Lett. **68**, 1351 (1992).

[30] K. D. Brommer, M. Needels, B. E. Larson, and J. D. Joannopoulos, Phys. Rev. Lett. **68**, 1355 (1992).

[31] M. S. Hybertsen and S. G. Louie, Phys. Rev. Lett. **55**, 1418 (1985).

[32] Y. Y. Zhang, W. G. Gao, S. Y. Chen, H. J. Xiang, and X.-G. Gong, Comput. Mater. Sci. **98**, 51 (2015).

[33] The exchange-correlation functional, the van der Waals density functional (vdW-DF) (optB86b-vdW functional) [34,35], which is capable of treating the dispersion force, is adopted. The electron-ion interaction is described by the projector augmented wave method [36], and a cutoff energy of 250 eV in the plane-wave basis set is used. A Monkhorst-Pack grid with a maximum spacing of $2\pi \times 0.02\,\text{Å}^{-1}$ is employed in the calculations. All atomic positions and lattice constants are optimized by using the conjugate gradient method where the total energy and atomic forces are minimized. The geometry optimization is performed until the remaining Hellmann-Feynman forces become less than 0.001 eV/Å to obtain the final structures.

[34] M. Dion, H. Rydberg, E. Schröder, D. C. Langreth, and B. I. Lundqvist, Phys. Rev. Lett. **92**, 246401 (2004).

[35] J. Klimeš, D. R. Bowler, and A. Michaelides, Phys. Rev. B **83**, 195131 (2011).

[36] P. E. Blöchl, Phys. Rev. B **50**, 17953 (1994).

[37] Phonon calculations are performed using the force-constant method as implemented in the PHONOPY program with forces calculated by VASP.

[38] See Supplemental Material at http://link.aps.org/supplemental/10.1103/PhysRevB.92.201413 for figures displaying geometrical and electronic structures, phonon dispersions, and optical properties for the multilayer silicene.

[39] STM images are simulated by calculating the local electron density of states following the Tersoff-Hamann approach: J. Tersoff and D. R. Hamann, Phys. Rev. B **31**, 805 (1985).

[40] A Si layer is defined following the convention of the silicene layer, i.e., a single bilayer layer, consisting of two Si atoms at the upper positions and the remaining two Si atoms at the lower positions in the 2×1 lateral cell of the Si(111) surface.

[41] M. Zitzlsperger, R. Honke, P. Pavone, and U. Schröder, Surf. Sci. **377**, 108 (1997).

[42] ABN is defined as N_{bond}/n, where N_{bond} and n are the total number of Si-Si chemical bonds (with the Si-Si distance being smaller than 2.7 Å) and Si atoms in silicene, respectively.

[43] AEBA is defined as $1 - [\sum_{i=1}^{N_{\text{angle}}} |A - \text{Ang}(i)|]/(AN_{\text{angle}})$, where N_{angle} and $\text{Ang}(i)$ are the total number of bond angles and the value of the ith bond angle in silicene, respectively. AEBA1 and AEBA2 correspond to $A = 109.47^\circ$ and 120°, respectively.

[44] W. Shockley and H. J. Queisser, J. Appl. Phys. **32**, 510 (1961).